Breathable Vapor Toxicant Barriers Based on Multilayer Graphene Oxide

Ruben Spitz Steinberg, Michelle Cruz, Naser G. A. Mahfouz, Yang Qiu, Robert H. Hurt[*]

School of Engineering, Brown University, Providence, RI 02912, United States

[*] Corresponding author email: robert_hurt@brown.edu

Supporting Information

Section S1. Film fabrication details.

GO suspensions were characterized using transmission electron microscopy (TEM) and atomic force microscopy (AFM) showing monolayer flakes with 1μm lateral dimensions and 1-2nm thickness (**Figure 1a,e**). The GO suspension was further characterized *via* x-ray photoelectron spectroscopy (XPS) and Raman spectroscopy (**Figure 1b,c**), both revealing a C:O atomic ratio of 2.1. GO films were prepared *via* positive pressure filtration[1] through a porous polycarbonate membrane; polycarbonate was chosen over anodized aluminum oxide in order to prevent crosslinking due to leached aluminum ions.[2] The thickness and number of layers for each GO film (δ_{GO} and n_{GO}) produced in this way were estimated using **eq S1** and e**q S2**:

$$\delta_{GO} = \frac{[GO]\, V_{GO}}{\rho_{GO} A_{PC}} \tag{S1}$$

$$n_{GO} = \frac{\delta_{GO}}{d_{GO}} \tag{S2}$$

where [GO] is the concentration of GO in suspension, V_{GO} is the volume of filtered suspension, ρ_{GO} is the density of GO,[3] A_{PC} is the filtration area of a track-etched polycarbonate support membrane (PC), and d_{GO} is the d-spacing for hydrated GO.[4-6]

To confirm the suitability of **eq S1** and **eq S2**, a film with a predicted thickness of 1μm was prepared and subsequently immersed in methylene chloride to dissolve the PC. AFM was used to study a piece of the resulting freestanding film, confirming the predicted thickness as seen in **Figure 1f**.

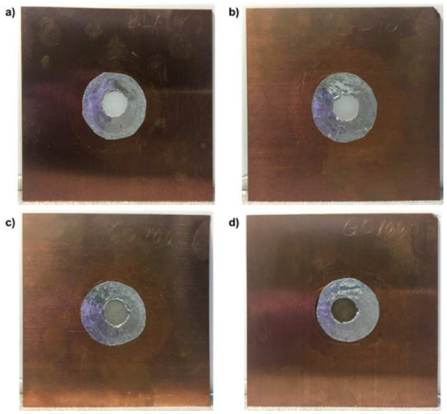

Figure S2. Representative photographs of molecular permeation GO samples. Details shown in Fig. 2 middle panel. (a) Assembly with only the track-etch polycarbonate support loaded; (b) including 10 nm GO film; (c) 100 nm GO film; (d) 1000 nm GO film.

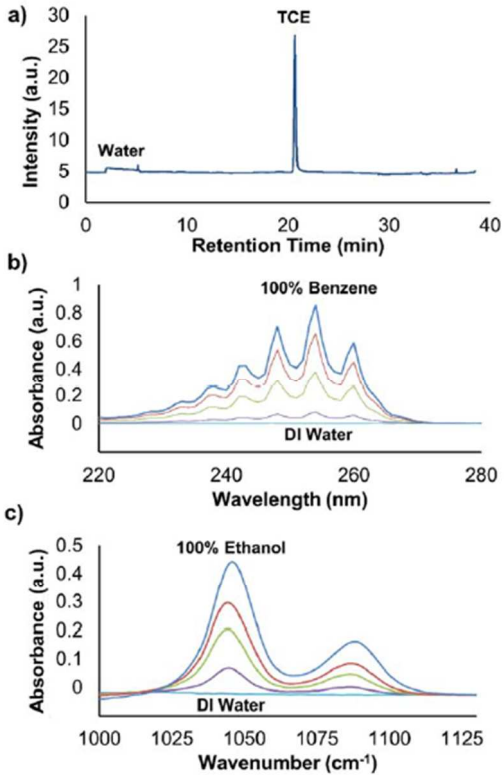

Figure S3. Analytical techniques used for determining aqueous toxicant concentrations. (a) A typical gas chromatograph for TCE in water, showing suitable separation. Calibration standards were used to develop a calibration curve based on TCE peak area; (b) UV-vis spectra for benzene in water at different concentrations, focusing on the linear extinction of the peak at 255 nm with decreasing benzene concentration; (c) FTIR spectra for ethanol in water at different concentrations, focusing on the C-O stretch peaks, which show linear extinction with decreasing ethanol concentration.

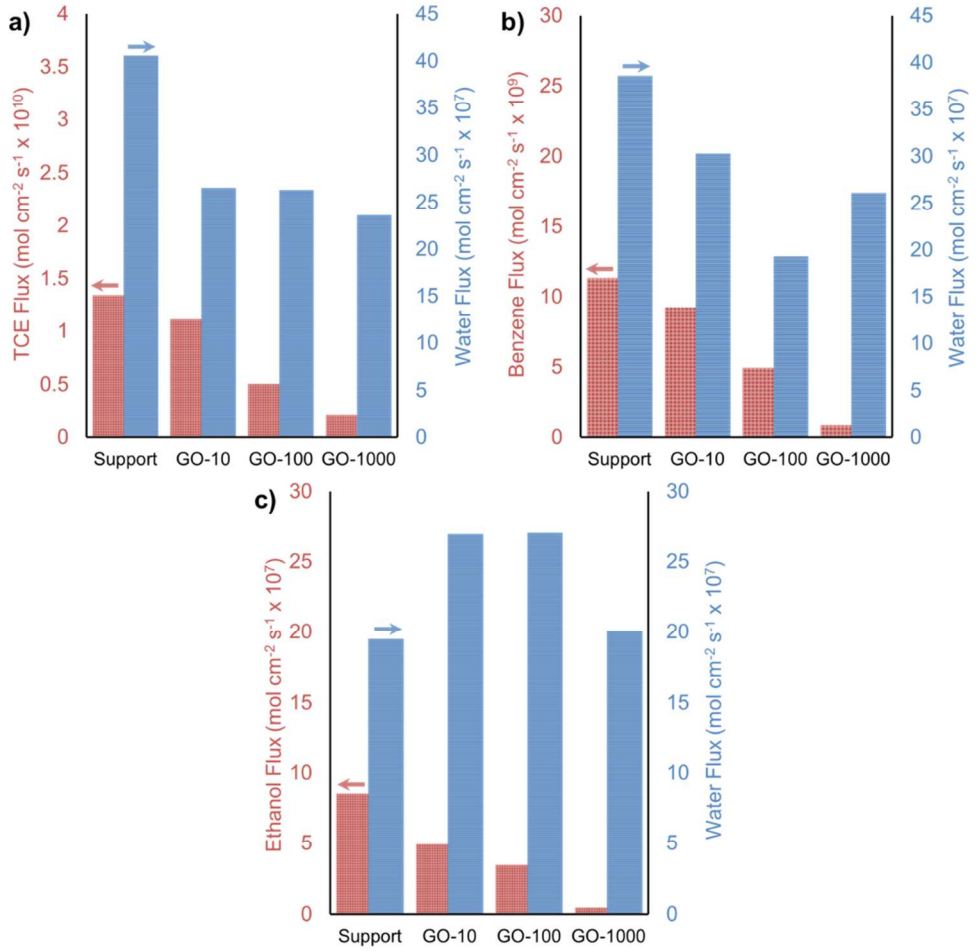

Figure S4. Flux and breathability results arranged by molecular permeant. (a) Simultaneous TCE flux and breathability. Note the three orders of magnitude difference in TCE transport (left axis) relative to water (right axis); (b) Simultaneous benzene flux and breathability. Note the two orders of magnitude difference in benzene transport (left axis) relative to water (right axis); (c) Simultaneous ethanol flux and breathability.

Section S5. Detailed derivation of transport models.

A one-dimensional steady-state mass conservation law was derived for a control-volume within the GO film with a convective component for water in one direction and a diffusive component for a compound, T, acting in the opposite direction.

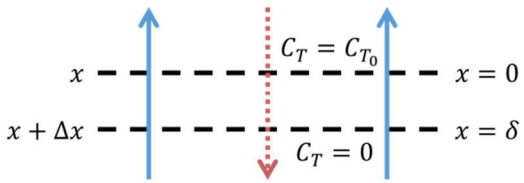

Balancing the inlets and outlets to the control volume between x and x+Δx leads to **eq S3**; grouping terms, dividing both sides by Δx, and taking the limit as Δx approaches zero leads to e**q S4**.

$$(v \cdot C_T)_{x+\Delta x} + \left(-D_{eff}\frac{dC_T}{dx}\right)_x = (v \cdot C_T)_x + \left(-D_{eff}\frac{dC_T}{dx}\right)_{x+\Delta x} \quad \text{(S3)}$$

$$-D_{eff}\frac{d^2C_T}{dx^2} = v\frac{dC_T}{dx} \quad \text{(S4)}$$

where C_T is the concentration of compound T in the film at x, D_{eff} is the effective diffusion coefficient of T in the GO film, and v is the velocity of water in the x-direction within the film. By keeping the water vapor side well mixed, the concentration of T at x = δ can be assumed to be near zero; the constant influx of toxicant vapor to the toxicant side fixes the concentration of T at x = 0 to some value, C_{T0}. These boundary conditions are presented as **eq S5**.

$$@x = 0,\ C_T = C_{T0};\quad @x = \delta,\ C_T = 0 \quad \text{(S5)}$$

Solving **eq S4** for C_T subject to the boundary conditions in e**q S5** yields an expression for C_T as a function of x. To obtain an expression for the flux of T, $\dot{N}_T$, one can conveniently choose

to evaluate flux at x = δ, where the convective term can be ignored because C_T = 0. The expression for the flux is then:

$$\dot{N}_T = \frac{C_{T0} v e^{-\left(\frac{v}{D_{eff}/\delta}\right)}}{1 - e^{-\left(\frac{v}{D_{eff}/\delta}\right)}} \tag{S6}$$

Equation S6 treats the film as a homogeneous phase. To make further progress we use a porous media approach that accounts for the existence of the impermeable nanosheets and the gallery spaces through which flow and diffusions occur. Because of the highly tortuous transport path and because only a fraction of the film thickness is available for transport, v is expected to be much larger than the superficial water velocity, v_s, and related as shown in eq S7. Similarly, the diffusion coefficient within the film is unknown and can be expected to be lower than the bulk diffusivity, D_B. Taking these additional criteria into account leads to a new expression, given as eq S8.

$$v = v_s \frac{\tau}{\theta}\,;\, D_{eff} = D \frac{\theta}{\tau} k \tag{S7}$$

$$\dot{N}_T = \frac{C_{T0} v_s \left(\frac{\tau}{\theta}\right) e^{-\left[\frac{v_s \left(\frac{\tau}{\theta}\right)^2}{D \cdot k} \delta\right]}}{1 - e^{-\left[\frac{v_s \left(\frac{\tau}{\theta}\right)^2}{D \cdot k} \delta\right]}} \tag{S8}$$

where v_s is the water velocity at the surface, τ is the pathway tortuosity, θ is the volume fraction available for transport, D is the true diffusivity of T in the hydrated channels within the GO film, and k is the aqueous-vapor partition coefficient for substance T.

This flux is also affected by mass transfer resistances inherent to the experimental setup and due to transport through the PC. To take these into account, it is necessary to use a mass transfer circuit[7] as outlined in **eq S9** and **eq S10.**

$$\dot{N}_T = K_{Total}\Delta C_T \tag{S9}$$

$$\frac{1}{K_{Total}} = \frac{1}{K_{Blank}} + \frac{1}{K_{GO}} \tag{S10}$$

where ΔC_T is the toxicant concentration gradient, K_{Total} is the total mass transfer conductance, K_{Blank} is the conductance inherent to the setup and PC, and K_{GO} is the conductance due to the presence of a GO film. K_{Blank} was found by determining $\dot{N}_{Blank}$ experimentally and K_{GO} was found using **eq S10**; each flux value was divided by ΔC_T to obtain corresponding K values.

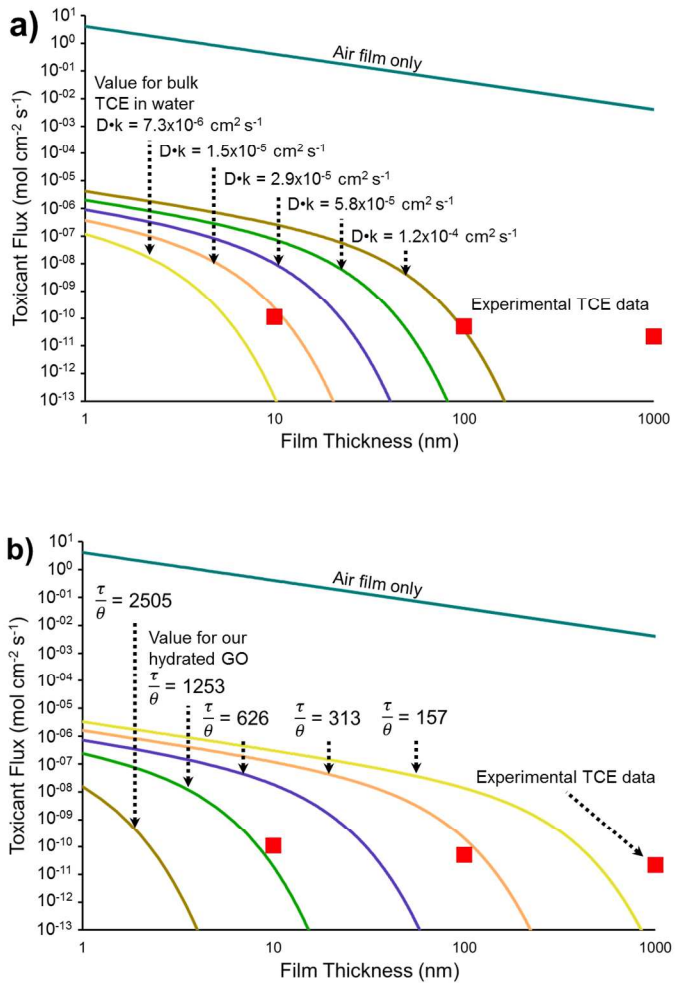

Figure S6. Permeation behavior predicted by simple model of homogeneous GO films. The model assumes uniform film properties and the diffusion of toxicant T through the gallery spaces only in counter-current to the water flow associated with active perspiration. The hypothetical flux through no film (a stagnant layer of air) is presented for comparison. The product of diffusivity and partition coefficient of the toxicant in water ($D \cdot k$) and the ratio of tortuosity and void fraction ($\frac{\tau}{\theta}$) were varied; the $D \cdot k$ value for TCE at 60°C and an estimate based on the Nielsen model for $\frac{\tau}{\theta}$ are highlighted. As $D \cdot k$ increases, a higher back-diffusive flux of toxicant can be expected, while increasing $\frac{\tau}{\theta}$ would lead to a lower back-diffusive toxicant flux; the model shows very high sensitivity to changes in both parameters as well as film thickness. Comparing the model to our experimental TCE data revealed completely different behaviors, leading to the conclusion that this model does not accurately describe the studied phenomenon.

Section S7. Details of comparison of our TCE permeabilities to those reported elsewhere. Both Sridhar and Tripathy[8] and McWatters and Rowe[9,10] reported diffusion coefficients for their studied materials. By dividing these reported coefficients by different film thicknesses, and by dividing our experimental fluxes by the corresponding concentration of TCE, we were able to obtain permeabilities for the sake of comparison. Note that McWatters and Rowe presented TCE and toluene data in their 2010 study, but only toluene data in their 2014 study. The relative TCE/toluene behavior reported in the former was used to estimate an expected TCE behavior in the latter.

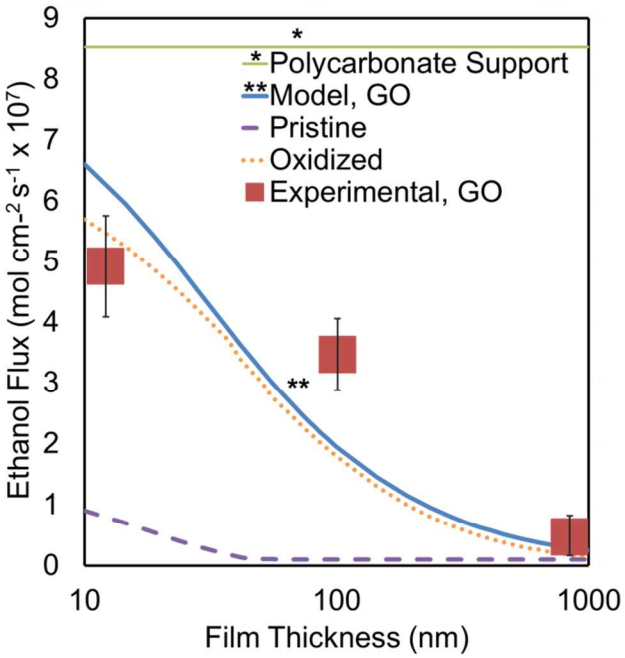

Figure S8. Model-data comparison for ethanol. The back-permeation of ethanol is thickness-dependent; the relative contributions of the pristine and oxidized pathways are presented.

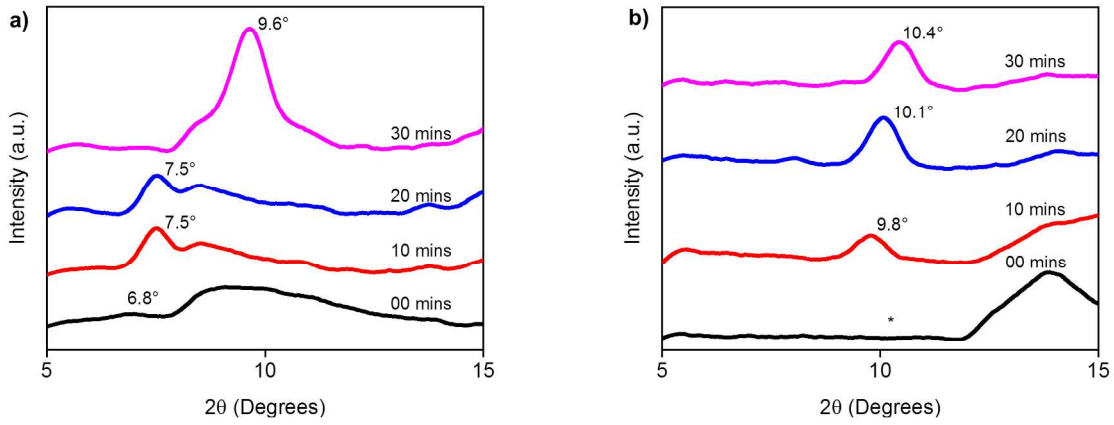

Figure S9. XRD analysis of GO films with interstitial liquids. GO films were soaked in water or ethanol and studied with an XRD during drying. (a) Water causes GO interlayer spacing to increase, as evidenced by the initial absence of the characteristic [001] peak. As water starts to evaporate and leave the interstitial spaces, the spacing between layers increase and the [001] peak appears at 7.5°. After 30 mins of drying, the [001] peak shifts to the right, indicating a further decrease in interlayer spacing; (b) Ethanol also spontaneously intercalates into GO films and causes swelling, with no visible [001] peak initially. As with water, ethanol evaporation causes a gradual decrease in the interlayer spacing. Consistent with other work, the d spacing is smaller when the interstitial liquid is ethanol instead of water.[6]

Supplementary References

1. Tang, Y. P.; Paul, D. R.; Chung, T. S., Free-Standing Graphene Oxide Thin Films Assembled by a Pressurized Ultrafiltration Method for Dehydration of Ethanol. *J Membr Sci* **2014,** *458*, 199-208.

2. Yeh, C. N.; Raidongia, K.; Shao, J. J.; Yang, Q. H.; Huang, J. X., On the Origin of the Stability of Graphene Oxide Membranes in Water. *Nat Chem* **2015,** *7*, 166-170.

3. Dikin, D. A.; Stankovich, S.; Zimney, E. J.; Piner, R. D.; Dommett, G. H. B.; Evmenenko, G.; Nguyen, S. T.; Ruoff, R. S., Preparation and Characterization of Graphene Oxide Paper. *Nature* **2007,** *448*, 457-460.

4. Acik, M.; Mattevi, C.; Gong, C.; Lee, G.; Cho, K.; Chhowalla, M.; Chabal, Y. J., The Role of Intercalated Water in Multilayered Graphene Oxide. *ACS Nano* **2010,** *4*, 5861-5868.

5. Mkhoyan, K. A.; Contryman, A. W.; Silcox, J.; Stewart, D. A.; Eda, G.; Mattevi, C.; Miller, S.; Chhowalla, M., Atomic and Electronic Structure of Graphene-Oxide. *Nano Lett* **2009,** *9*, 1058-1063.

6. Talyzin, A. V.; Hausmaninger, T.; You, S. J.; Szabo, T., The Structure of Graphene Oxide Membranes in Liquid Water, Ethanol and Water-Ethanol Mixtures. *Nanoscale* **2014,** *6*, 272-281.

7. Incropera, F. P., *Fundamentals of Heat and Mass Transfer*. John Wiley: **2007**.

8. Sridhar, V.; Tripathy, D. K., Barrier Properties of Chlorobutyl Nanoclay Composites. *J Appl Polym Sci* **2006,** *101*, 3630-3637.

9. McWatters, R. S.; Rowe, R. K., Diffusive Transport of VOCs Through LLDPE and Two Coextruded Geomembranes. *J Geotech Geoenviron* **2010,** *136*, 1167-1177.

10. McWatters, R. S.; Rowe, R. K. In *An Investigation of Toluene and TCE Diffusion Through EVOH in Aqueous Solutions*, 10th International Conference on Geosynthetics, Berlin, Germany, Berlin, Germany, September 21-25, **2014**.